Available online at www.sciencedirect.com

ScienceDirect

Nuclear Physics B 900 (2015) 431–445

NUCLEAR PHYSICS B

www.elsevier.com/locate/nuclphysb

Exclusive Higgs boson production through electromagnetic process in p–p and Pb–Pb ultra-peripheral collisions

Jia-Qing Zhu, Zhi-Lei Ma, Chao-Yi Shi, Yun-De Li *

Department of Physics, Yunnan University, Kunming 650091, People's Republic of China

Received 24 August 2015; received in revised form 25 September 2015; accepted 26 September 2015

Available online 1 October 2015

Editor: Stephan Stieberger

Abstract

The Higgs boson production through electromagnetic process in the exclusive p–p and Pb–Pb ultra-peripheral collisions is calculated. According to the condition of conference, the equivalent photon approximation formulation is used, and the limitations of the variables in the calculations are obtained. Three kinds of the equivalent photon spectrums are considered: the plane wave form, the approximate plane wave forms of Dress et al., and the semi-classical form. For comparison, the gluon–gluon fusion and intrinsic heavy flavors contributions are presented. The numerical results show that, the plane wave photon spectrum with correct limitations of the variables provides more reasonable results for the exclusive $p + p \to p + p + H$ and $Pb + Pb \to Pb + Pb + H$ processes, and the electromagnetic process provides meaningful contributions for the exclusive Higgs production in ultra-peripheral collisions.

1. Introduction

Ultra-peripheral collisions (UPCs) [1–4] are such reactions that two ions do not interact directly with each other but interact via their photons cloud. Based on the method of Fermi [5], Weizsäcker [6] and Williams [7], the moving electromagnetic fields of charged particles can be

* Corresponding author.
E-mail address: yndxlyd@163.com (Y.-D. Li).

http://dx.doi.org/10.1016/j.nuclphysb.2015.09.023

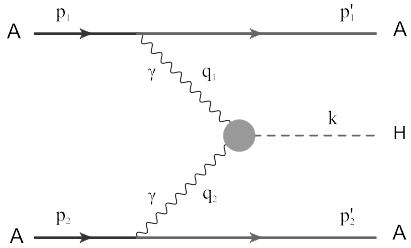

Fig. 1. An illustration for the exclusive Higgs boson production in UPCs, where p_i $(i = 1, 2)$ is the colliding nucleus momentum, p_i' is the scattered nucleus momentum, $q_i = p_i - p_i'$ is the virtual photon momentum, k is the Higgs boson momentum.

treated as a flux of virtual photons. In an ultra-relativistic ion collider, these photons can interact with target nucleus in the opposing beam (photoproduction) or with the photons of the opposing beam (two-photon reactions). At the Large Hadron Collider (LHC) energies, the intense heavy-ion beams represent a prolific source of quasi-real photons, hence it enables extensive studies of UPCs physics.

Since a Higgs boson was discovered at LHC in 2012 [8] and examined in 2013 [9], it spurs greater interest for further detailed studies of its properties, both in theory and experiment. In this paper, we investigate the production of the Standard Model Higgs boson (H) through two-photon reactions in p–p and Pb–Pb UPCs. Particularly, we are interested in the exclusive $p + p \to p + p + H$ and $Pb + Pb \to Pb + Pb + H$ processes which the colliding nuclei are intact and even non-excited. For these reactions, the coherence condition [1,10] limits the virtuality of the photons to very low values, and therefore the Weizsäcker–Williams approach or the equivalent photon approximation formulation can be used to study this topic.

In the next section, we clarify the reasonable of the equivalent photon approximation formulation in the study of the exclusive $p + p \to p + p + H$ and $Pb + Pb \to Pb + Pb + H$ processes. According to the coherence condition, we obtain the kinematic limits of the variables in our calculation. Section 3 presents three kinds of the photon spectrum functions: the plane wave form, the approximate plane wave form, and the semi-classical impact parameter form. The differences among these photon spectrums are discussed. In Section 4, the cross section of $\gamma + \gamma \to H$, described by the so-called transition form factor, is introduced, and the numerical results for the total cross sections of $p + p \to p + p + H$ and $Pb + Pb \to Pb + Pb + H$ are presented. In Section 5, we compare our results with the diffractive Higgs productions from the gluon–gluon fusion and intrinsic heavy flavors in p–p ultra-peripheral collisions. In Section 6 we summarize our work.

2. Formulation of the exclusive UPCs

The cross section for exclusive Higgs boson production in UPCs through electromagnetic process (see Fig. 1) can be expressed as follows [11]:

$$d\sigma = \frac{(4\pi\alpha)^2}{4Q_1^2Q_2^2\sqrt{(p_1p_2)^2 - m_1^2m_2^2}}\rho_1^{\mu\mu'}\rho_2^{\nu\nu'}M^*{}_{\mu'\nu'}M_{\mu\nu}d\mathrm{PS}_3(p_1, p_2; p_1', p_2', k), \tag{1}$$

where

$$d\mathrm{PS}_3(p_1, p_2; p_1', p_2', k) = (2\pi)^4\delta^4(q_1 + q_2 - k)\frac{d^3p_1'}{(2\pi)^3 2E_1}\frac{d^3p_2'}{(2\pi)^3 2E_2}\frac{d^3k}{(2\pi)^3 2k_0}, \tag{2}$$

$M^{\mu\nu}$ is the amplitude of reaction $\gamma^*+\gamma^* \to H$, p_i $(i=1,2)$ is the colliding nucleus momentum, $s=(p_1+p_2)^2$, $\sqrt{s}=2E$ is the total c.m.s. energy, p_i' is the scattered nucleus momentum, $E_i=p_i'^0$ is the scattered nucleus energy, $m_i^2=p_i^2=p_i'^2=m_A^2$, $q_i=p_i-p_i'$ is the virtual photon momentum, $q_i^2=-Q_i^2<0$, k is the Higgs boson momentum. For convenient, we define $y_i=\omega_i/E$, where $\omega_i=E-E_i$ in c.m.s. The generalized density-matrix of a virtual photon with non-polarized initial and final nuclei is

$$\begin{aligned}\rho_i^{\mu\nu} &= 2m_i W_i^{\mu\nu} \\ &= -\left(g^{\mu\nu}-\frac{q_i^\mu q_i^\nu}{Q_i^2}\right)C_i(Q_i^2)+\frac{(2p_i-q_i)^\mu(2p_i-q_i)^\nu}{Q_i^2}D_i(Q_i^2),\end{aligned} \tag{3}$$

where

$$\begin{aligned}C(Q^2) &= 2m_A W_1, \\ D(Q^2) &= \nu W_2=\frac{Q^2}{2m_A}W_2.\end{aligned} \tag{4}$$

The minimum value of Q_i^2 is

$$Q_{i\,\min}^2=\frac{\omega_i^2}{\gamma_L^2(1-\omega_i/E)}=\frac{y_i^2}{1-y_i}m_A^2, \tag{5}$$

where γ_L is the Lorentz boost of a single beam which has a simple form in colliding nuclei c.m.s.

$$\gamma_L=\frac{E}{m_A}. \tag{6}$$

In the exclusive $p+p\to p+p+H$ and $Pb+Pb\to Pb+Pb+H$ reactions, the nuclei are intact and non-excited after scattering, which means the wavelength of the photon is larger than the size of the nucleus, and all the charged constituents inside the nucleus should act coherently. The condition for coherence, which limits the virtuality Q^2 of the photon to very low value, can be expressed as [1,10]

$$Q^2\le\frac{1}{R_A^2}, \tag{7}$$

where the size of the nucleus is

$$R_A=A^{1/3}1.2\ \text{fm}. \tag{8}$$

Therefore, we get the maximum value for Q^2

$$Q_{i\,\max}^2=Q_{\max}^2=A^{-2/3}0.027\ \text{GeV}^2. \tag{9}$$

Since $Q_{i\,\min}^2<Q_{i\,\max}^2$, the maximum value of y_i can be obtained as

$$y_{i\,\max}=y_{\max}=\sqrt{\frac{1}{4}\left(\frac{Q_{\max}^2}{m_A^2}\right)^2+\frac{Q_{\max}^2}{m_A^2}}-\frac{1}{2}\frac{Q_{\max}^2}{m_A^2}. \tag{10}$$

From Eq. (9) and Eq. (10), we have

For p–p UPCs,

$$y_{\max}|_p = 0.160,$$
$$Q^2_{\max}|_p = 0.027\ \text{GeV}^2. \tag{11}$$

For Pb–Pb UPCs,

$$y_{\max}|_{Pb^{206}} = 1.423 \times 10^{-4},$$
$$Q^2_{\max}|_{Pb^{206}} = 7.655 \times 10^{-4}\ \text{GeV}^2. \tag{12}$$

The total c.m.s. energy for $\gamma^* + \gamma^* \to H$ is defined as

$$\hat{s} = (q_1 + q_2)^2 = m_H^2. \tag{13}$$

Since $Q^2_{\max} \ll \hat{s}$, $\hat{s} \approx y_1 y_2 s$, and

$$y_{i\,\min} = \frac{m_H^2}{y_{\max} s}. \tag{14}$$

On the other hand, according to $y_{i\,\min} < y_{i\,\max}$, the minimum value of $\sqrt{s}$ for the exclusive UPCs can be obtained as

$$\sqrt{s}|_{\min} = \frac{m_H}{y_{\max}}, \tag{15}$$

where

$$\sqrt{s}|_{p\,\min} = 788\ \text{GeV} \quad \text{for p–p UPCs},$$
$$\sqrt{s_{NN}}|_{Pb^{206}\,\min} = 4350\ \text{GeV} \quad \text{for Pb–Pb UPCs}. \tag{16}$$

Finally, because of the very low value of Q_i^2, the equivalent photon approximation (EPA) [11–13] can be used for the exclusive $p + p \to p + p + H$ and $Pb + Pb \to Pb + Pb + H$ reactions, and Eq. (1) can be rewritten (with azimuthal averaging) as

$$d\sigma = \sigma_{\gamma\gamma} dn_1 dn_2, \tag{17}$$

where $\sigma_{\gamma\gamma}$ is the sub-cross section for the $\gamma + \gamma \to H$ that the photons are on mass shell. The expression in Eq. (17) is the essence of the EPA for the two-photon production, where dn_i is the number of equivalent photons, or the photon spectrum.

3. The photon spectrum

For the exclusive electromagnetic processes where the nucleus is intact after the emission of photon, there are some different photon spectrum forms in the literatures [14–22]. In this paper, we will consider three of them and compare their results for the Higgs-boson production in p–p and Pb–Pb UPCs.

3.1. The plane wave form

The plane wave form of the photon spectrum can be obtained directly from Eqs. (1)–(2). By using

$$\frac{d^3p_1'}{E_1}\frac{d^3p_2'}{E_2} = \frac{\pi^2 s}{(p_1p_2)^2 - m_1^2m_2^2} dQ_1^2 dQ_2^2 d\omega_1 d\omega_2, \tag{18}$$

and define

$$R^{\mu\nu} = -g^{\mu\nu} + \frac{(q_1q_2)(q_1^\mu q_2^\nu + q_2^\mu q_1^\nu) - q_1^2 q_2^\mu q_2^\nu - q_2^2 q_1^\mu q_1^\nu}{(q_1q_2)^2 - q_1^2q_2^2},$$
$$\rho_i^{++} = \frac{1}{2} R_{\mu\nu}\rho_i^{\mu\nu}, \tag{19}$$

the EPA spectrum in Eq. (17) can be presented as

$$\begin{aligned} dn_i &= \frac{\alpha}{2\pi}\rho_i^{++}\frac{\omega_i d\omega_i dQ_i^2}{E^2Q_i^2} \\ &= \frac{\alpha}{\pi}\frac{d\omega_i}{\omega_i}\frac{dQ_i^2}{Q_i^2}\left[\left(1-\frac{\omega_i}{E}\right)\left(1-\frac{Q_{i\,\min}^2}{Q_i^2}\right)D_i(Q_i^2) + \frac{\omega_i^2}{2E^2}C_i(Q_i^2)\right] \\ &= \frac{\alpha}{\pi}\frac{dy_i}{y_i}\frac{dQ_i^2}{Q_i^2}\left[(1-y_i)\left(1-\frac{Q_{i\,\min}^2}{Q_i^2}\right)D_i(Q_i^2) + \frac{1}{2}y_i^2 C_i(Q_i^2)\right]. \end{aligned} \tag{20}$$

The thorough discussion can be found in Ref. [11]. For the p–p case, C_i and D_i, associated with the form factors, can be expressed as

$$C(Q^2)_p = \mu_p^2 G_E^2(Q^2),$$
$$D(Q^2)_p = \frac{4m_p^2 + \mu_p^2 Q^2}{4m_p^2 + Q^2} G_E^2(Q^2). \tag{21}$$

In the consideration region of Q^2, G_E can be parametrized precisely by the dipole form

$$G_E(Q^2) = G_D(Q^2) = \left(1 + \frac{Q^2}{0.71\ \text{GeV}^2}\right)^{-2}. \tag{22}$$

For the Pb–Pb case, since $\omega_i \ll E$ ($y_{i\,\max} \ll 1$, see Eq. (11) and Eq. (12)), the coefficient in front of C_i is small which is neglected in our calculation, and $D(Q^2)_{Pb}$ can be presented as

$$D(Q^2)_{Pb} = Z^2 F(Q^2)_{Pb}^2. \tag{23}$$

The charge form factor $F(Q^2)$ is the Fourier transform of the charge density ρ of the nucleus,

$$F(Q^2) = \frac{\pi}{4}\int_0^\infty r\rho(r)\sin(qr)dr, \tag{24}$$

where ρ is parametrized by the two-parameter Fermi (2pF) model [23]:

$$\rho(r)_{Pb^{206}}^{2\text{pF}} = \frac{\rho_0}{1 + \exp\left(\frac{r - 6.61\ \text{fm}}{0.545\ \text{fm}}\right)}, \tag{25}$$

and by treating the proton as a point-like particle for Pb, we have

$$\rho_0 = 0.08\ \text{proton/fm}^3. \tag{26}$$

Inserting Eqs. (25)–(26) into Eq. (24), one finds that [17]

$$F(Q^2)^2_{Pb} \approx \exp\left(-\frac{Q^2}{Q_0^2}\right) \tag{27}$$

in the region of $Q \leq 120$ MeV, where $Q_0 = 55$–60 MeV. The comparisons of the different Q_0 choices with the "exact" result inferred from Eq. (24) and Eq. (25) directly can be found in [17]. In this paper, we chose $Q_0 = 60$ MeV since $y_{\max}|_{Pb^{206}} \approx 10^{-4}$.

3.2. The approximate plane wave form

For many cases, an approximation of the plane wave photon spectrum form is quite reasonable and is useful for estimates. In Ref. [18], Drees and Zeppenfeld provided a useful approximate analytic expression of Eq. (20), which is widely used in the literatures. By setting

$$\begin{aligned} &C(Q^2)_p \approx D(Q^2)_p \approx G_E^2(Q^2), \\ &Q_i^2 - Q_{i\,\min}^2 \approx Q_i^2, \end{aligned} \tag{28}$$

and integrating Q_i^2 from $Q_{i\,\min}^2$ to $Q_{i\,\max}^2 = \infty$, Eq. (20) becomes

$$\begin{aligned} \frac{dn_i|_p^{D.Z}}{dy_i} &= \frac{\alpha}{\pi y_i} \int\limits_{Q_{i\,\min}^2}^{\infty} \frac{dQ_i^2}{Q_i^2}\left[(1-y_i)\left(1-\frac{Q_{i\,\min}^2}{Q_i^2}\right)D_i(Q_i^2) + \frac{1}{2}y_i^2 C_i(Q_i^2)\right] \\ &= \frac{\alpha}{\pi}\frac{1-y_i+\frac{1}{2}y_i^2}{y_i} \int\limits_{Q_{i\,\min}^2}^{\infty} \frac{dQ_i^2}{Q_i^2} G_E^2(Q^2) \\ &= \frac{\alpha}{2\pi}\frac{1+(1-y_i)^2}{y_i}\left[\ln A - \frac{11}{6} + \frac{3}{A} - \frac{3}{2A^2} + \frac{1}{3A^2}\right], \end{aligned} \tag{29}$$

where

$$A = 1 + \frac{0.71\ \text{GeV}^2}{Q_{\min}^2}. \tag{30}$$

It can be seen that, the important characteristic of Eq. (29) is that the maximum value of Q_i^2 is chosen as ∞, which means $y_{i\,\max} = 1$ (see Eq. (10)), and $\sqrt{s}|_{\min}$ in Eq. (15) tends to m_H. These will be the possible error source when Eq. (29) is used to the calculation of $p + p \to p + p + H$.

A similar result for Pb^{206} is calculated by Dress, Ellis and Zeppenfeld in Ref. [17] by using the form factor in Eq. (27):

$$\frac{dn_i|_{Pb^{206}}^{D.E.Z}}{dy_i} = \frac{\alpha}{\pi}\left[-\frac{\exp\left(-Q_{i\,\min}^2/Q_0^2\right)}{y_i} + \left(\frac{1}{y_i} + \frac{m_i^2}{Q_0^2}y_i\right)\Gamma\left(0, Q_{i\,\min}^2/Q_0^2\right)\right], \tag{31}$$

where the incomplete Gamma Function

$$\Gamma(a,z) = \int\limits_z^{\infty} t^{a-1}e^{-t}dt. \tag{32}$$

Again, $Q_{i\,\max}^2 = \infty$, $y_{i\,\max} = 1$ and $\sqrt{s}|_{\min} = m_H$.

3.3. The semiclassical form

Another most important approach for the photon spectrum is the semiclassical impact parameter description, which excludes the hadronic interaction easily. The calculation of the semiclassical photon spectrum for the case of E1 (electric dipole) excitations is explained in Ref. [24] and the result is

$$dn_i|^{s.c.}_{\mathrm{E1}} = \frac{2Z^2\alpha}{\pi}\left(\frac{c}{\upsilon}\right)^2\frac{d\omega_i}{\omega_i}\left[\xi K_0K_1 + \frac{\xi^2}{2}\left(\frac{\upsilon}{c}\right)^2\left(K_0^2 - K_1^2\right)\right], \tag{33}$$

where υ is the velocity of the point charge Ze, $K_0(x)$ and $K_1(x)$ are the modified Bessel functions,

$$\xi = \frac{\omega_i b_{\min}}{\gamma_L\upsilon} = \frac{b_{\min}m_A}{\upsilon}y_i. \tag{34}$$

$b_{\min} = R_1 + R_2$ for the UPCs. In this paper, we use $b_{\min} = 2R_p$ for the p–p case and $2R_{Pb}$ for the Pb–Pb case.

Since $\gamma_L \gg 1$ in p–p and Pb–Pb UPCs in LHC, the inclusion of other multipolarities of excitation is also important. The most important two are the magnetic dipole M1 and the electric quadrupole E2 cases which can be found in Refs. [14–16]

$$dn_i|^{s.c.}_{\mathrm{E2}} = \frac{2Z^2\alpha}{\pi}\left(\frac{c}{\upsilon}\right)^4\frac{d\omega_i}{\omega_i}\left[2\left(1-\frac{\upsilon^2}{c^2}\right)K_1^2 + \xi\left(2-\frac{\upsilon^2}{c^2}\right)^2 K_0K_1 + \frac{\xi^2}{2}\left(\frac{\upsilon}{c}\right)^4\left(K_0^2 - K_1^2\right)\right], \tag{35}$$

$$dn_i|^{s.c.}_{\mathrm{M1}} = \frac{2Z^2\alpha}{\pi}\frac{d\omega_i}{\omega_i}\left[\xi K_0K_1 + \frac{\xi^2}{2}\left(K_0^2 - K_1^2\right)\right]. \tag{36}$$

It can be seen that, since $\upsilon \approx 1$ in ultra-relativistic UPCs,

$$\begin{aligned} dn_i|^{s.c.} &= dn_i|^{s.c.}_{\mathrm{E1}} + dn_i|^{s.c.}_{\mathrm{E2}} + dn_i|^{s.c.}_{\mathrm{M1}} \\ &= 3dn_i|^{s.c.}_{\mathrm{E1}} \\ &= \frac{6Z^2\alpha}{\pi}\frac{d\omega_i}{\omega_i}\left[\xi K_0K_1 + \frac{\xi^2}{2}\left(K_0^2 - K_1^2\right)\right]. \end{aligned} \tag{37}$$

Although the semi-classical photon spectrum is Q^2-independent, the limitations of its variable y are also the same as Eq. (11) and Eq. (12) due to the coherence condition.

4. Numerical results and discussions for the electromagnetic process

The Higgs boson production through the reaction $\gamma^* + \gamma \to H$ (see Fig. 2) was investigated by Gabrielli, Ilyin and Mele [25,26], and the recent works [27,28] have confirmed their computation. For the exclusive $p + p \to p + p + H$ and $Pb + Pb \to Pb + Pb + H$ cases, only the amplitude that the photons are on mass shell is needed in the EPA formulation. The cross section for $\gamma + \gamma \to H$ expressed by the "transition form factor" can be found in Ref. [27]. In this formulation, $\sigma_{\gamma\gamma}$ in Eq. (17) can be expressed as

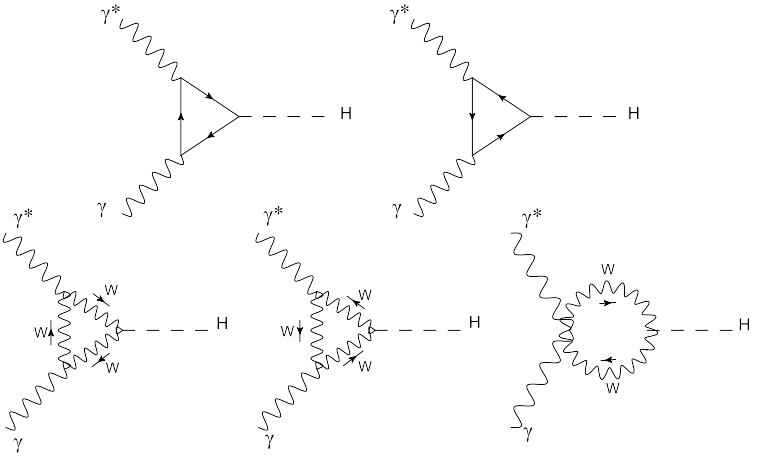

Fig. 2. Fermion triangle-loop contribution and W boson loop contribution for $\gamma^* + \gamma \to H$ [27].

$$\sigma_{\gamma\gamma} = \left(M^*{}_{\mu\nu} M^{\mu\nu}\right)_{Q^2=0} \frac{(2\pi)^4 \delta^4(q_1 + q_2 - k)}{4\sqrt{(p_1 p_2)^2 - m_1^2 m_2^2}} \frac{d^3k}{(2\pi)^3 2k_0}, \tag{38}$$

where

$$M^{\mu\nu} = \frac{ge^2}{(4\pi)^2 m_W} \left(g^{\mu\nu} q_1 \cdot q_2 - q_2^\mu q_1^\mu\right) F_{\text{total}}, \tag{39}$$

$e = \sqrt{4\pi\alpha_{em}}$ and $g = \sqrt{8G_F m_W^2/\sqrt{2}}$ are the electromagnetic and weak gauge couplings, respectively, m_W is the W boson mass, and G_F is the Fermi coupling constant. The transition form factor F_{total} is defined as:

$$F_{\text{total}} = \sum_f N_c e_f^2 F_{1/2} + F_1, \tag{40}$$

where $F_{1/2}$ and F_1 are contributions from fermion loops and W boson loops (Fig. 2), respectively. Since $F_{1/2}$ is proportions to the fermion mass squared m_f^2, the contributions from leptons and light-flavor quarks are negligibly small compared to the top quark. Therefore only the top quark loop contribution is considered in this paper. Taking $Q^2 \to 0$, one can obtain

$$\begin{aligned} F_{1/2}|_{Q^2=0} &= -2\tau_t \left[1 + (1-\tau_t)\sin^{-2}\sqrt{\frac{1}{\tau_t}}\right], \\ F_1|_{Q^2=0} &= 2 + 3\tau_W + 3\tau_W(2-\tau_W)\sin^{-2}\sqrt{\frac{1}{\tau_W}}, \end{aligned} \tag{41}$$

where

$$\tau_t = \frac{4m_t^2}{m_H^2}, \qquad \tau_W = \frac{4m_W^2}{m_H^2}. \tag{42}$$

By using

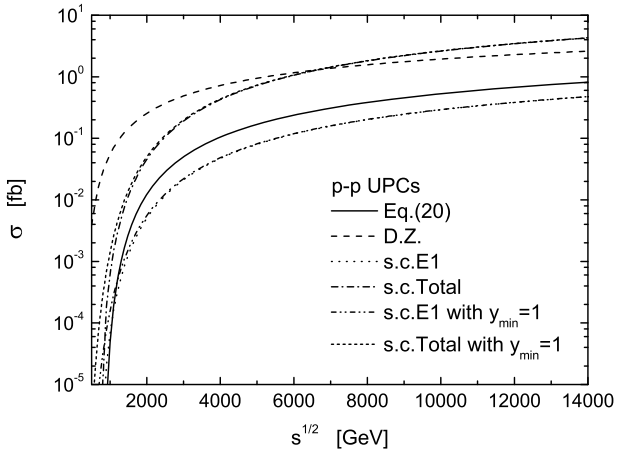

Fig. 3. The numerical results for the total cross sections of $p + p \to p + p + H$ with different photon spectrums.

$$\frac{1}{2k_0} = \int dk_0 \delta(k^2 - m_H^2)\theta(k_0^2), \tag{43}$$

we get

$$\sigma_{\gamma\gamma} = \pi S_1^2|_{Q^2=0}\delta(\hat{s} - m_H^2). \tag{44}$$

Inserting Eq. (44) into Eq. (17), the numerical results for exclusive $p + p \to p + p + H$ and $Pb + Pb \to Pb + Pb + H$ processes are illustrated in Fig. 3 and Fig. 4. Both of the two processes we compare calculations of the four different equivalent photon spectrums, where the mass parameters and the coupling constants are chosen as [29]

$$\begin{aligned} &m_W = 80.385\ \text{GeV}, \qquad m_t = 173.21\ \text{GeV}, \qquad m_H = 125.7\ \text{GeV}, \\ &m_p = 0.938\ \text{GeV}, \qquad G_F = 1.166 \times 10^{-5}\ \text{GeV}^2. \end{aligned} \tag{45}$$

The solid lines present the results of the plane wave form in Eq. (20), the dash lines indicate the contributions of the approximate plane wave form in Eq. (29) for p–p UPCs (D.Z.) and Eq. (31) for Pb–Pb UPCs (D.E.Z.), the dot lines illustrate the data of the electric dipole excitations of semi-classical photon spectrum in Eq. (33) (s.c.E1), and the dash dot lines present the total results of E1, E2 and M1 semi-classical photon spectrum in Eq. (37) (s.c.Total). Both of the two semi-classical ones above are calculated with the same limitations of the variables ($y_{\min}$ and $y_{\max}$). For comparison, we also calculate the semi-classical photon spectrums with $y_{\max} = 1$ (corresponding to the choice of $Q^2_{\max} = \infty$): the electric dipole excitation ones are denoted by the dash dot dot lines (s.c.E1 with $y_{\max} = 1$), and the total ones are illustrated by the short dash lines (s.c.Total with $y_{\max} = 1$). It can be seen that,

1. Eq. (20) provides negative values in the $\sqrt{s}$ region smaller than $\sqrt{s}|_{\min}$ (see Eq. (16)), while the approximate plane wave ones are always positive when $\sqrt{s}$ is larger than m_H. These differences can also be seen for the semi-classical ones with different $y_{\max}$ choices. The semi-classical forms with correct $y_{\max}$ (s.c.E1 and s.c.Total) doesn't have meaningful results when $\sqrt{s} < \sqrt{s}|_{\min}$, while the ones with $y_{\max} = 1$ are always positive when $\sqrt{s}$ is larger than m_H. This means that, when $\sqrt{s} < \sqrt{s}|_{\min}$, the approximate plane wave photon spectrums (Dress–Zeppenfeld in Eq. (29) and Dress–Ellis–Zeppenfeld in Eq. (31)) and the semi-classical ones with incorrect $y_{\max}$ will provide erroneous results for the exclusive Higgs boson production in p–p

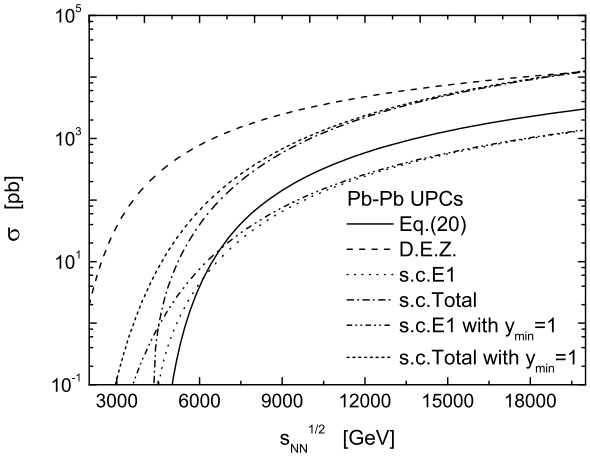

Fig. 4. The same as Fig. 3 but for $Pb + Pb \to Pb + Pb + H$.

and Pb–Pb UPCs. The reason is that, although the photon spectrums decrease rapidly with the increasing Q^2, incorrect $Q^2_{\max}$ value will cause incorrect threshold of $\sqrt{s}$.

2. In the region of $\sqrt{s} > \sqrt{s}|_{\min}$, the differences between the two $y_{\max}$ choices of the semi-classical results become so small. The contributions of Eq. (20) are somewhat higher than the semi-classical E1 results but lower than the other cases (for Pb–Pb UPCs in the LHC region that $\sqrt{s_{NN}} \leq 5.5$ TeV, the semi-classical E1 photon spectrum provides higher contributions than the ones of Eq. (20)). The approximate plane wave results (Dress–Zeppenfeld and Dress–Ellis–Zeppenfeld) are higher than the others for the small $\sqrt{s}$, and become smaller than the total results of E1, E2 and M2 semi-classical photon spectrum at large $\sqrt{s}$. From Fig. 3 and Fig. 4 we can see that, although the differences among them will become small at sufficient large $\sqrt{s}$, the results of the approximate plane wave photon spectrums are about an order of magnitude larger than the ones of the plane wave form and the semi-classical E1 form in the present experimental $\sqrt{s}$ region.

5. Comparisons with the productions from gluon–gluon fusion and intrinsic heavy flavors

In the literatures, two important mechanisms for the Higgs production in the exclusive reaction $p + p \to H$ are developed: the gluon–gluon fusion process and the intrinsic heavy flavors contribution. In this section, we compare the electromagnetic result with these two mechanisms.

The gluon–gluon fusion process is illustrated in Fig. 5, where two hard gluons couple to the Higgs ($gg \to H$), and a third gluon is also exchanged in order that both protons remain color singlet. The most quoted and first calculation for this process is done in the Khoze, Martin and Ryskin (KMR) model [30]. Another useful approach is developed by Cudell, Dechambre, Hernández and Ivanov [31], which is similar to the KMR model but differs in the implementation and details. In this paper, we use the KMR model for the discussion.

In the KMR model, the cross section is assumed to factorize between the effective luminosity $\mathcal{L}$ and the hard subprocess $\hat{\sigma}$ [32]

$$\sigma^{gg} = \mathcal{L} \times \hat{\sigma}^{\text{excl}}(gg \to H)$$

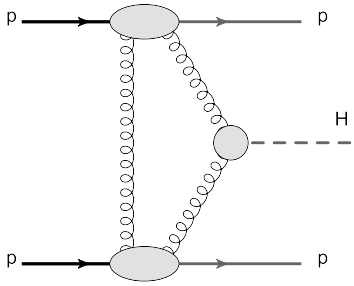

Fig. 5. The gluon–gluon fusion process for the Higgs exclusive production in p–p UPCs.

$$= \int dy \int dM^2 \frac{\partial \mathcal{L}}{\partial y \partial M^2} \hat{\sigma}^{\text{excl}}(gg \to H), \tag{46}$$

where the hard subprocess cross section is

$$\hat{\sigma}^{\text{excl}}\left(gg^{PP} \to H\right) \approx \delta \left(1 - \frac{M^2}{m_H^2}\right) 1.1 \text{ pb}, \tag{47}$$

and the luminosity has the form

$$\frac{\partial \mathcal{L}}{\partial y \partial M^2} = M^{-2} \hat{S}^2 L, \tag{48}$$

where the "soft" survival factor $\hat{S}^2$ can be found in Ref. [33]. To single log accuracy, we have

$$L = \left[\frac{\pi}{8b} \int \frac{dQ_t^2}{Q_t^4} f_g\left(x_1, x_1', Q_t^2, \mu^2\right) f_g\left(x_2, x_2', Q_t^2, \mu^2\right)\right]^2, \tag{49}$$

where b is the t-slope corresponding to the momentum transfer distributions of the colliding protons and is chosen as 4 GeV^{-2}, Q_t is the virtuality of the screening gluon. The qualities $f_g\left(x, x', Q_t^2, \mu^2\right)$ is the generalized (skewed) unintegrated gluon density of the proton which can be presented as the simplified form

$$f_g\left(x, x', Q_t^2, \mu^2\right) = R_g \frac{\partial}{\partial \ln Q_t^2}\left[\sqrt{T(Q_t, \mu)} x g\left(x, Q_t^2\right)\right], \tag{50}$$

where $g\left(x, Q_t^2\right)$ is the conventional integrated gluon density, $\mu = m_H/2$ is the hard scale, $R_g \approx 1.2$, $x \approx m_H/\sqrt{s}$ [34], the Sudakov factor is ($\Delta = k_t/(\mu + k_t)$)

$$T(Q_t, \mu) = \exp\left(-\int_{Q_t^2}^{\mu^2} \frac{\alpha_S\left(k_t^2\right)}{2\pi} \frac{dk_t^2}{k_t^2} \int_0^{1-\Delta} \left[z P_{gg}(z) + \sum_q P_{qg}(z)\right] dz\right). \tag{51}$$

The intrinsic heavy flavors mechanism (see Fig. 6) to the exclusive Higgs production in p–p UPCs is based on the assumption of the presence of intrinsic heavy quark (IQ) fluctuations in the proton bound state. The detailed discussion about this mechanism can be found in Ref. [35]. The cross section for intrinsic charm contribution is

$$\sigma^{\text{IC}} = \frac{32}{\pi^2} \frac{G_F P_{\text{IC}}}{z_0} \frac{m_c^4}{m_H^4} \frac{\left[\sigma_{\text{tot}}^{\pi p}(\tilde{s})\right]^2}{B(\tilde{s}) \left\langle r_{\text{ch}}^2 \right\rangle_p} \frac{\gamma^2(\tilde{s})}{\left[2 + 2\gamma(\tilde{s}) + \gamma^2(\tilde{s})\right]^3} \left[1 + \frac{\left\langle r_{\text{ch}}^2 \right\rangle_p}{16 \left\langle r_{\text{ch}}^2 \right\rangle_\pi} \frac{1}{\gamma(\tilde{s})}\right]^2$$

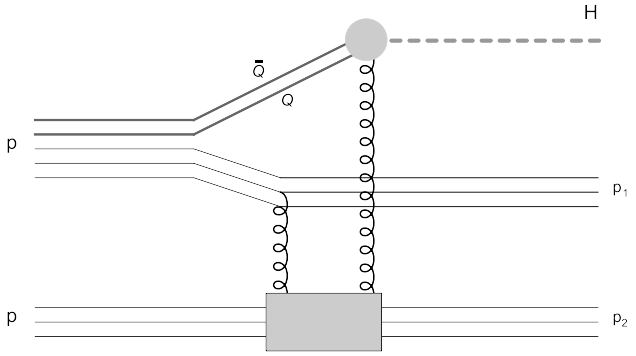

Fig. 6. The intrinsic heavy flavors contribution for the Higgs exclusive production in p–p UPCs.

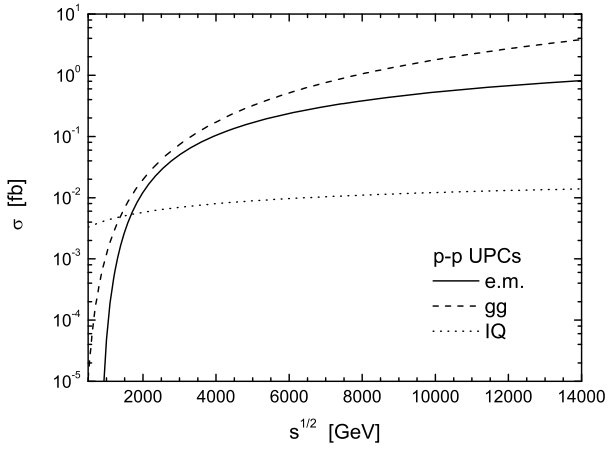

Fig. 7. The comparisons between the total cross sections of the electromagnetic, gluon–gluon fusion and intrinsic heavy flavors contributions for the Higgs exclusive production in p–p UPCs.

$$\times \left[\beta\sqrt{\frac{\omega}{2m_c}} + \sqrt{1-\beta^2}\ln\left(\frac{m_H}{2m_c}\right)\right]^2. \tag{52}$$

An analogous expression can be used for the intrinsic bottom case. For top quark in the proton,

$$\sigma^{\mathrm{IT}} = \frac{8}{\pi^2}\frac{G_F P_{\mathrm{IT}}}{z_0}\frac{m_t^4}{m_H^4}\frac{\left[\sigma_{\mathrm{tot}}^{\pi p}(\tilde{s})\right]^2}{B(\tilde{s})\langle r_{\mathrm{ch}}^2\rangle_p}\frac{\gamma^2(\tilde{s})}{\left[2+2\gamma(\tilde{s})+\gamma^2(\tilde{s})\right]^3}\left[1+\frac{\langle r_{\mathrm{ch}}^2\rangle_p}{16\langle r_{\mathrm{ch}}^2\rangle_\pi}\frac{1}{\gamma(\tilde{s})}\right]^2$$
$$\times\left[1+\frac{1-\delta}{\delta}\ln(1-\delta)\right]^2. \tag{53}$$

Including the absorptive corrections, the cross sections become

$$\tilde{\sigma}^{\mathrm{IQ}} = \sigma^{\mathrm{IQ}}\left\{1-\frac{1}{\pi}\frac{\sigma_{\mathrm{tot}}^{pp}(\tilde{s})}{B(\tilde{s})+2B_{\mathrm{el}}^{pp}(\tilde{s})}+\frac{1}{(4\pi)^2}\frac{\left[\sigma_{\mathrm{tot}}^{pp}(\tilde{s})\right]^2}{B_{\mathrm{el}}^{pp}(\tilde{s})\left[B(\tilde{s})+B_{\mathrm{el}}^{pp}(\tilde{s})\right]}\right\}. \tag{54}$$

Parameters in the above equations are chosen as [35,36]

$$\omega = 0.3\ \text{GeV},\ P_{\text{IC}} = 0.01,\ P_{\text{IQ}} = \frac{P_{\text{IC}} m_c^2}{m_Q^2},\ \delta = \frac{m_H^2}{4m_t^2},$$

$$\tilde{s} = \frac{s z_0 M_0^2}{M_H^2},\ z_0 = 0.75,\ M_0 = 1\ \text{GeV},\ s_0 = 1000\ \text{GeV}^2,$$

$$\left\langle r_{\text{ch}}^2 \right\rangle_p = 0.79\ \text{fm}^2,\ \left\langle r_{\text{ch}}^2 \right\rangle_\pi = 0.44\ \text{fm}^2,$$

$$B(s) = B_0 + 2\alpha'_{\text{P}} \ln\left(\frac{s}{M_0^2}\right),\ B_0 = 4\ \text{GeV}^{-2},\ \alpha'_{\text{P}} = 0.25\ \text{GeV}^{-2},$$

$$B_{\text{el}}^{pp}(s) = B_{\text{el}}^0\left(1 + 0.067 \ln\left(s/M_0^2\right)\right),\ B_{\text{el}}^0 = 7.5\ \text{GeV}^{-2},$$

$$\gamma(s) = \frac{R_p^2}{4R_0^2(s)},\ R_p^2 = \frac{2}{3}\left\langle r_{\text{ch}}^2 \right\rangle_p,\ R_0^2(s) = 0.88\ \text{fm} \times \left(\frac{s}{s_0}\right)^{-0.14},$$

$$\sigma_{\text{tot}}^{\pi p}(s) = 23.6\ \text{mb} \times \left(\frac{s}{s_0}\right)^{0.08},\ \sigma_{\text{tot}}^{pp}(s) = 21.8\ \text{mb} \times \left(\frac{s}{M_0^2}\right)^{0.08},$$

and we use $m_c = 1.275$ GeV, $m_b = 4.18$ GeV and $m_t = 173.5$ GeV [29] for the calculations.

The total cross sections of the gluon–gluon fusion (gg) and intrinsic heavy flavors (IQ) contributions to the Higgs exclusive production in p–p UPCs are illustrated in Fig. 7. For comparison, we also present the electromagnetic (e.m.) contribution according to Eq. (20). It can be seen that,

1. The gluon–gluon fusion is always larger than the other two mechanisms. Including the present theoretical uncertainty for the KMR model (see the discussions in Ref. [37]), contribution of the electromagnetic process is comparable with the gluon–gluon fusion in the region of $\sqrt{s} >$ 1000 GeV.

2. The result of gluon–gluon fusion falls fast with the decreasing of $\sqrt{s}$, and the intrinsic heavy flavors mechanism will dominate the exclusive Higgs production in the small $\sqrt{s}$ region.

The $d\sigma/dx_F$ for the different mechanisms as a function of the Higgs x_F are also presented. The Feynman x, which is defined as $x_F = x_1 - x_2$, denotes the longitudinal momentum fraction carried by the Higgs boson (see Ref. [32], and $x_2 - x_1$ is used to denote the longitudinal momentum fraction of the Higgs boson in Ref. [35]). For the electromagnetic process, one can use y_1 and y_2 as the longitudinal momentum fractions x_1 and x_2 since $Q^2 \to 0$. The numerical results for p–p UPCs with $\sqrt{s} = 7$ TeV and $\sqrt{s} = 14$ TeV are illustrated in Fig. 8, where the $x_F > 0$ region is considered. It can be seen that,

1. The electromagnetic process dominates the exclusive Higgs boson production in p–p UPCs at small x_F region. However, due to the limitation of y_{max}, the electromagnetic process is invalid when $x_F > 0.16$. By comparison, the electromagnetic mechanism provides effective results in the whole x_F region if the approximate plane wave spectrum or the semi-classical form is used for the calculation.

2. The gluon–gluon fusion contributions are larger than the ones of intrinsic heavy flavors at small x_F region. The crossover point of the two mechanism at $x_F \approx 0.025$ for $\sqrt{s} = 7$ TeV and $x_F \approx 0.175$ for $\sqrt{s} = 14$ TeV. The intrinsic heavy flavors mechanism dominates the exclusive Higgs boson production in p–p UPCs at large x_F region.

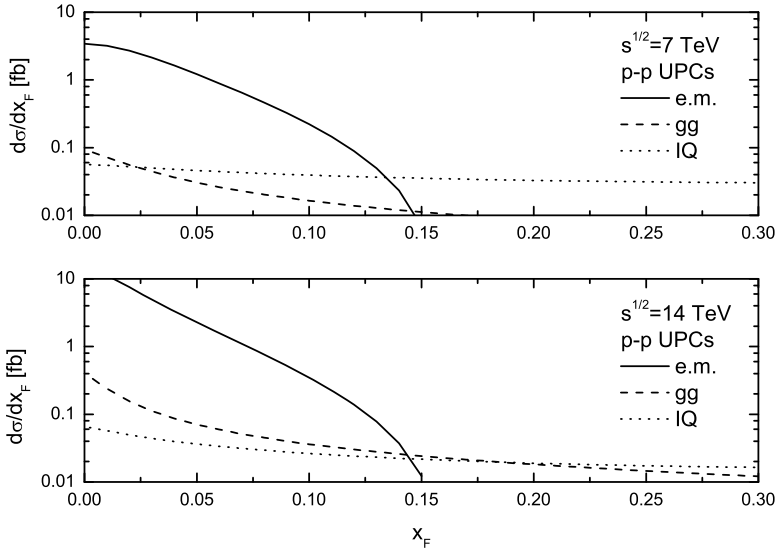

Fig. 8. The comparisons between $d\sigma/dx_F$ of the electromagnetic, gluon–gluon fusion and intrinsic heavy flavors contributions for the Higgs exclusive production in p–p UPCs.

6. Conclusion

In this paper, we calculate the Higgs boson production in the exclusive $p + p \to p + p + H$ and $Pb + Pb \to Pb + Pb + H$ reactions through electromagnetic process. Since the condition of conference restricts the maximum virtuality $Q^2_{\max}$ of the virtual photon to very low value, the Weizsäcker–Williams approach or the equivalent photon approximation formulation can be used in the calculations. Three kinds of the equivalent photon spectrums are considered in the present work: the plane wave form (see Eq. (20)), the approximate plane wave forms (see Eq. (29) and Eq. (31)), and the semi-classical form (see Eq. (33) and Eq. (37)).

Due to the small value of $Q^2_{\max}$, the kinematic limits of the variables ($y_{\max}$, $y_{\min}$ and $\sqrt{s}|_{\min}$) can be obtained for the calculations of the plane wave form and the semi-classical form. On the other hand, $Q^2_{\max}$ is chosen as ∞ in the approximate plane wave forms (Dress–Zeppenfeld and Dress–Ellis–Zeppenfeld) and the semi-classical ones with $y_{\max} = 1$, the threshold of $\sqrt{s}$ is reduced to m_H, which will cause the erroneous results when $\sqrt{s}$ is less than $\sqrt{s}|_{\min}$ in Eq. (15). In the region of $\sqrt{s} > \sqrt{s}|_{\min}$, the contributions of the plane wave forms are somewhat higher than the semi-classical E1 results but much lower than the ones of the approximate wave forms and the total (E1 + E2 + M2) semi-classical ones. It can be seen that, the plane wave photon spectrum in Eq. (20) provides more reasonable results for the exclusive $p + p \to p + p + H$ and $Pb + Pb \to Pb + Pb + H$ processes, and the appropriate limitations of the variables (especially $Q^2_{\max}$) is important for the computations.

The comparisons between our results with the gluon–gluon fusion and intrinsic heavy flavors contributions in p–p ultra-peripheral collisions are also presented. For the total cross sections, the electromagnetic process is comparable with the gluon–gluon fusion in the region of $\sqrt{s} >$ 1000 GeV, and the intrinsic heavy flavors mechanism dominate the exclusive Higgs production in the small $\sqrt{s}$ region. For the $d\sigma/dx_F$, the electromagnetic mechanism provides the most important contribution when $x_F < 0.16$, and the intrinsic heavy flavors mechanism dominates

the exclusive Higgs boson production in p–p UPCs at large x_F region. The electromagnetic process provides meaningful contributions for the exclusive Higgs production in ultra-peripheral collisions.

Acknowledgements

This work is supported by the National Natural Science Foundation of China under Grant Nos. 11065010 and 11465021.

References

[1] G. Baur, et al., Phys. Rep. 364 (2002) 359.
[2] C.A. Bertulani, S.P. Klein, J. Nystrand, Annu. Rev. Nucl. Part. Sci. 55 (2005) 271.
[3] J. Nystrand, Nucl. Phys. A 787 (2007) 29c.
[4] A.J. Baltz, et al., Phys. Rep. 458 (2008) 1.
[5] E. Fermi, Z. Phys. 29 (1924) 315.
[6] C.F.V. Weizsäcker, Z. Phys. 88 (1934) 612.
[7] E.J. Williams, Phys. Rev. 45 (1934) 729.
[8] ATLAS Collaboration, Phys. Lett. B 716 (2012) 1;
CMS Collaboration, Phys. Lett. B 716 (2012) 30.
[9] ATLAS Collaboration, Phys. Lett. B 726 (2013) 88;
ATLAS Collaboration, Phys. Lett. B 726 (2013) 120;
CMS Collaboration, Phys. Rev. Lett. 110 (2013) 081803.
[10] G. Baur, K. Hencken, D. Trautmann, J. Phys. G 24 (1998) 1657.
[11] V.M. Budnev, I.F. Ginzburg, G.V. Meledin, V.G. Serbo, Phys. Rep. 15 (1975) 181.
[12] S.J. Brodsky, T. Kinoshita, H. Terazawa, Phys. Rev. D 4 (1971) 1532.
[13] H. Terazawa, Rev. Mod. Phys. 45 (1973) 615.
[14] A. Winther, K. Alder, Nucl. Phys. A 319 (1979) 518.
[15] C.A. Bertulani, G. Baur, Nucl. Phys. A 442 (1985) 739.
[16] C.A. Bertulani, G. Baur, Nucl. Phys. A 458 (1986) 725.
[17] M. Drees, J. Ellis, D. Zeppenfeld, Phys. Lett. B 223 (1989) 454.
[18] M. Drees, D. Zeppenfeld, Phys. Rev. D 39 (1989) 2536.
[19] E. Papageorgiu, Phys. Lett. B 250 (1990) 155.
[20] B.A. Kniehl, Phys. Lett. B 254 (1991) 267.
[21] S. Frixione, M.L. Mangano, P. Nasonm, G. Ridolfi, Phys. Lett. B 319 (1993) 339.
[22] J. Nystrand, Nucl. Phys. A 752 (2005) 470c.
[23] C.W. de Jager, H. de Vries, C. de Vries, At. Data Nucl. Data Tables 14 (1974) 479;
H. de Vries, C.W. de Jager, C. de Vries, At. Data Nucl. Data Tables 36 (1987) 495.
[24] J.D. Jackson, Classical Electrodynamics, Wiley, New York, 1975.
[25] E. Gabrielli, V.A. Ilyin, B. Mele, Phys. Rev. D 56 (1997) 5945.
[26] E. Gabrielli, V.A. Ilyin, B. Mele, Phys. Rev. D 60 (1999) 113005.
[27] N. Watanabe, Y. Kurihara, K. Sasaki, T. Uematsu, Phys. Lett. B 728 (2014) 202.
[28] N. Watanabe, Y. Kurihara, T. Uematsu, K. Sasaki, Phys. Rev. D 90 (2014) 033015.
[29] K.A. Olive, et al., Particle Data Group, Chin. Phys. C 38 (2014) 090001.
[30] V.A. Khoze, A.D. Martin, M.G. Ryskin, Eur. Phys. J. C 14 (2000) 525.
[31] J.R. Cudell, A.D. Dechambre, O.F. Hernández, I.P. Ivanov, Eur. Phys. J. C 61 (2009) 369.
[32] V.A. Khoze, A.D. Martin, M.G. Ryskin, Eur. Phys. J. C 23 (2002) 311.
[33] V.A. Khoze, A.D. Martin, M.G. Ryskin, Eur. Phys. J. C 18 (2000) 167.
[34] V.A. Khoze, A.D. Martin, M.G. Ryskin, Eur. Phys. J. C 19 (2001) 477.
[35] S.J. Brodsky, B. Kopeliovich, I. Schmidt, J. Soffer, Phys. Rev. D 73 (2006) 113005.
[36] B. Kopeliovich, A. Schäfer, A. Tarasov, Phys. Rev. D 62 (2000) 054022.
[37] A. Dechambre, O. Kepka, C. Royon, R. Staszewski, Phys. Rev. D 83 (2011) 054013.